An Efficient Filter Bank Structure for Adaptive Notch Filtering and Applications

Wenyi Wu, Yegui Xiao, Jianhui Lin, Liying Ma, Khashayar Khorasani

自适应陷波滤波器（ANF）和自适应陷波滤波器组（ANFB）

***Abstract*—Second-order IIR adaptive notch filters (ANF) and banks (ANFB) have been extensively utilized in many applications ranging from biomedical engineering to control systems. In this paper, a new efficient ANFB is proposed that is composed of two filter banks, namely a prefilter bank with cascaded IIR notch filters and a parallel structure IIR ANFB. The second-order IIR ANFs or filter bank cells in the proposed ANFB are updated by utilizing a modified normalized gradient (ModNG) algorithm. The proposed ANFB requires the same number of cells as does a conventional parallel form ANFB. However, the filter weight initialization drawback that the conventional parallel form ANFB inherently suffers from is significantly alleviated in the proposed ANFB. Equipped with the ModNG algorithm, the proposed ANFB yields considerably improved frequency estimation performance as compared to the conventional parallel form ANFB, for a wide range of frequencies and signal-to-noise ratios (SNR). Furthermore, preliminary steady-state analysis is provided for both the proposed and conventional ANFBs, which significantly enhances our understanding of their capabilities and features. Extensive case study simulations are conducted to demonstrate the superiority of the proposed ANFB over the conventional parallel form ANFB. The proposed ANFB is also applied to real noise and vibration signals to reveal its promising analytical and practical capabilities.**

***Index Terms*—Adaptive notch filter (ANF), Adaptive notch filter bank (ANFB), Second-order IIR ANF, Normalized gradient (NG) algorithm, Signal-to-noise ratio (SNR), Frequency estimation and tracking.**

I. Introduction

DETECTION and enhancement of sinusoidal signals is a very basic and important problem in many signal processing applications [1]. Examples range from biomedical engineering to control systems, including active noise control, power engineering, digital communications, among many others. In the 1970s and early 1980s, the adaptive line enhancer (ALE) was widely investigated, that aims at enhancing sinusoids corrupted by additive noise through estimating and tracking unknown sinusoidal frequencies [1]-[3]. The ALE is based on the use of an FIR filter and a gradient-based or Gauss-Newton algorithm. It is computationally involved mainly due to the polynomial rooting that is required in the frequency identification process. To improve the performance of ALE, extensive attempts based on IIR-type adaptive notch filters (ANF), bandpass filter or other filter structures have been made [4]-[25]. These efforts have revealed that the ANF has significant computational advantages in terms of the frequency estimation and tracking as compared to the ALE. In this paper, our focus is concentrated on the ANF and the ANF banks (ANFB).

Corresponding author: xiao@pu-hiroshima.ac.jp, Tel: +81-82-251-9731, FAX: +81-82-251-9405. W. Wu and J. Lin are with the Southwest Jiaotong University, Chengdu, China, Y. Xiao is with the Prefectural University of Hiroshima, Hiroshima, Japan, and L. Ma and K. Khorasani are with the Concordia University, Montreal, Canada.

In adaptive IIR notch filtering, three typical IIR notch filters have been proposed and extensively studied. They are the second-order IIR ANF with constrained poles and zeros [5], the lattice-type IIR ANF [6], [7], and the bilinear second-order ANF [8]. A number of adaptive algorithms have been developed for these ANFs in the literature. Typical and known algorithms including the recently proposed ones are the sign algorithm (SA) [9] and its modified version (modified SA (MSA)) [17], the plain gradient algorithm (PG) [10] and its modified version (unbiased PG (UPG) [18]), the p-power algorithm [13], the memoryless nonlinear gradient algorithm (MNG) [14], the normalized gradient algorithm (NG) [8]-[10], the recursive prediction error algorithm (RPE) [4], [5], among others. These algorithms, except the RPE, have been developed solely for the second-order IIR ANFs that can estimate and track a single frequency involved in a sinusoidal signal that contains one or multiple sinusoids. Recent algorithm development and application exploration may be found in [19]-[32], including several technically demanding algorithmic trials as well as some very interesting applications.

To process signals that include multiple sinusoids, one needs to adopt a bank of second-order IIR ANFs, i.e., an ANFB. Each cell or section in the ANFB is a single second-order ANF that corresponds to a single frequency or sinusoid. Three typical ANFBs have been developed in the literature. The first ANFB was proposed by Rao and Kung that designate it as "cascade implementation of an adaptive notch filter" [4]. It represents a cascade-form second-order IIR notch filter bank. Given that its cells are adapted individually (AI), it was called as an AI structure in [15]. Here, it is called cascade ANFB (CANFB). It has p cells, where p denotes the number of frequencies that the CANFB is expected to target and track. The second ANFB was proposed by Kwan and Martin [8], and was referred to as a triangular cascade ANF (TCANFB) [7]. Given that its end cells are adapted simultaneously (AS), it was also denoted as an AS structure in [15]. The total number of cells that are utilized is $\frac{1}{2}p(p+1)+(p-1)$. Obviously, the TCANFB requires significantly more cells than the CANFB. Each TCANFB end cell is updated after the other frequency components are all reduced from its input. This implies that the operating conditions of TCANFB updated cells tend to be uniform as far as the input SNR is concerned. The major drawback of the TCANFB is its complexity due to the number of cells that are included. On the contrary,

the cells in the CANFB scheme operate in different SNR environment, with the first cell suffers from the poorest SNR as all the sinusoids remain in its input, whereas the last cell enjoys the most favorable input where all other sinusoids are significantly reduced. Therefore, the frequency estimation bias in the CANFB scheme tends to be larger than that of the TCANFB [15].

To mitigate the shortcomings associated with the CANFB and TCANFB schemes, Pei and Tseng had proposed a new parallel structure ANFB [15]. It is a parallelly pre-filtered and parallelly updated ANFB (PPANFB). Only $2p$ cells are included in the PPANFB, with p cells placed in parallel as a pre-filter bank and the other p cells also allocated and updated in parallel. Its complexity is twice that of the CANFB, but considerably smaller than that of the TCANFB. It is shown theoretically and confirmed by extensive simulation studies that the PPANFB is comparable to the TCANFB in terms of frequency estimation performance [15]. Unfortunately, the PPANFB suffers from a serious drawback, namely the initial weights or filter coefficients of the parallel updated cells must be well placed to allow each updated cell to eventually target different frequencies. In other words, if a segment of prior information on the signal frequency distribution is unavailable, one may be unable to place the initial weights properly and some or all of the PPANFB updated cells may target the same frequency, rendering the filter bank useless. The initialization issue with the PPANFB poses a major limitation that considerably reduces its applicability in real applications. In the past two decades, to the best of our knowledge, no effort has been made in developing new ANFB to overcome drawbacks and limitations of the above mentioned three ANFBs.

In this paper, we propose a new efficient ANFB that consists of two filter banks, namely a cascade form notch pre-filter bank and a parallel form ANFB. It is a cascade pre-filtered and parallel updated ANFB (CPANFB). A modified normalized gradient (ModNG) algorithm is introduced to update the filter weights corresponding to the updated or active cells. The proposed CPANFB has the same number of cells that the conventional PPANFB has, however it basically does not suffer from the filter weight initialization problem. Moreover, the proposed CPANFB that is equipped with the ModNG presents significantly improved frequency estimation and tracking performance as compared to the conventional PPANFB that is updated by conventional NG, over wide ranges of frequency and SNR. Preliminary steady-state analysis is conducted for the existing and proposed ANFBs. Extensive simulations are presented to show the effectiveness of the proposed CPANFB. Application of the proposed CPANFB to real noise and vibration signals is also conducted in order to reveal its promising analytical capabilities and achievable performance in comparisons with the conventional PPANFB.

文章框架

The remainder of this paper is organized as follows. Section 2 presents four (4) ANFBs, namely the CANFB, the TCANFB, the PPANFB, and the proposed ANFB. In the same section, a modified NG (ModNG) algorithm is proposed for updating the proposed ANFB and preliminary steady-state analysis are provided for the 4 ANFBs. Extensively simulation and comparative studies are conducted and demonstrated in Section 3. In Section 4, the proposed CPANFB is applied to real noise and vibration signals to demonstrate and verify its applicabilities and capabilities. Section 5 concludes the paper.

II. A New ANFB

噪声 or 振动信号 x(n)

The noise or vibration signal $x(n)$ to be analyzed contains p sinusoids that are contaminated by an additive noise signal $v(n)$,

要分析的噪声或振动信号x(n)包含p个正弦波，这些正弦波被加性噪声信号v(n)污染，

$$\begin{aligned} x(n) &= \sum_{i=1}^{p} A_i \cos(\omega_i n + \theta_i) + v(n) \\ &= \sum_{i=1}^{p} s_i(n) + v(n) \end{aligned} \tag{1}$$

where A_i, ω_i and θ_i denote respectively the amplitude, the angular frequency and the phase of the i-th sinusoid $s_i(n)$, and $v(n)$ denotes a zero-mean additive white Gaussian noise (AWGN) with variance σ^2. If p is equal to 1 or only a single sinusoid with frequency ω is included in $x(n)$, a second-order ANF may be used to estimate that frequency. A typical second-order IIR ANF with constrained poles and zeros [5] is expressed by

什么意思？

$$H_{\rm N}(z) = \frac{1 + cz^{-1} + z^{-2}}{1 + \rho c z^{-1} + \rho^2 z^{-2}} \tag{2}$$

where $\rho \in [0, 1)$ denotes a pole attraction parameter that defines the notch bandwidth as well as the pole radius, c $(= -2\cos\omega_0)$ denotes a filter coefficient or weight that is updated to converge to $-2\cos\omega$, the variable ω_0 is called the notch frequency that will be very close to the signal frequency ω when ANF converges and reaches to its steady state. The selection of ρ is very important, due to the fact that ρ presents significant influence on not only the dynamics but also the steady-state properties of the ANF [5], [10], [13], [15]-[19], [33]. Selection over a range $[0.90, 0.99]$ usually leads to satisfactory results in most practical applications.

ρ 的建议取值范围

If multiple sinusoids are embedded in $x(n)$, an ANFB is required for estimating and tracking t second-order IIR ANF in the ANFB pr or cell. In the past four decades, several typical ANFB have been proposed and applied in the literature such as [4], [7], [8], and [15].

An ANFB cell is shown in Fig. 1. In the cell, the input comes in from the left, the notch filter output goes out from the right, the gradient signal with respect to the filter weight or coefficient appears on the top, and the bandpass signal is shown on the bottom. The bandpass filter transfer function is derived from the notch filter (2) and given by

$$\begin{aligned} H_{\rm B}(z) &= 1 - H_{\rm N}(z) \\ &= -(1-\rho)z^{-1}\frac{c + (1+\rho)z^{-1}}{1 + \rho c z^{-1} + \rho^2 z^{-2}}. \end{aligned} \tag{3}$$

A. Conventional ANFBs

Three typical and conventional ANFBs are shown in Fig. 2, where active cell bodies are indicated by thick squares. The

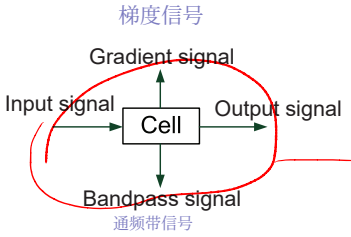

Fig. 1 The schematic of the ANFB cell.

first one is the CANFB (Fig. 2(a)) [4] whose p active cells are adapted individually. The SNR at the input of cells are not the same. That is to say, the cells operate under different SNR conditions. The first or the leftmost cell yields the worst result as its input contains all sinusoids as well as additive noise during the entire adaptation process. The last or the rightmost cell works under the most favorable SNR condition as its input consists of additive noise and sinusoid(s) that are not suppressed by other cells to its left. On the other hand, the first cell tends to converge to a given frequency faster than the cells on its right, and convergence of the last cell tends to be the slowest. Therefore, CANFB cells do not converge at the same pace, which is not a desirable property. The most attractive merit of CANFB is that it only requires p cells, each cell eventually converging to a different frequency regardless of setting the initial cell weights.

The second ANFB (Fig. 2(b)) is the TCANFB [7], [8]. The number of cells is $\frac{1}{2}p(p+1)+(p-1)$, which may become significantly larger than that of the CANFB if $p \gg 1$. The SNR at the input of active cells tends to be similar, since all the sinusoids except the one being targeted are removed by the $p-1$ pre-filtering cells to its left. Therefore, the p active cells on the rightmost of TCANFB tend to converge in a similar manner, each targeting a different frequency as the adaptation process approaches to the steady state no matter what the cell weights are initially set to.

The third ANFB is the PPANFB (Fig. 2(c)) [15]. It requires only $2p$ cells, with p active cells on the rightmost are adapted simultaneously. Clearly, the number of cells is twice that of the CANFB, however it is considerably less than that of TCANFB. Extensive simulations conducted have shown that the PPANFB filter weights present quite the same convergent behavior if their initial values are well set and spaced. This is because all PPANFB active cells operate under similar SNR conditions. It is also shown theoretically that the PPANFB enjoys quite the same steady-state performance that the TCANFB could provide [15]. However, this ANFB suffers from a significant disadvantage as compared to the CANFB and TCANFB. Specifically, the initial cell weights must be properly selected and spaced with respect to the target frequencies. If all the initial cell weights are set to zero, the same frequency will be targeted by all the active cells. Some of the active cells may actually target the same frequency even if their initial values are set differently. For all active cells to capture different frequencies, their initial weights must be set different and properly spaced. To ensure this, information on distribution of frequencies is required in advance. Obviously, this requirement may pose significant challenges and limitations in real applications.

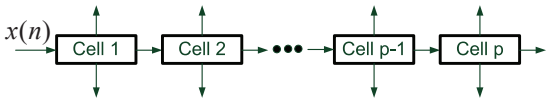

(a) The CANFB [4].

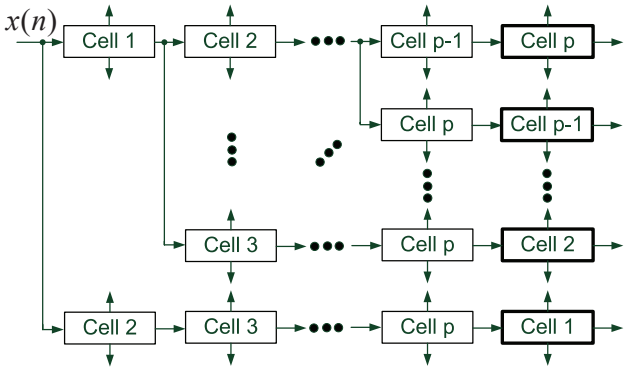

(b) The TCANFB [8].

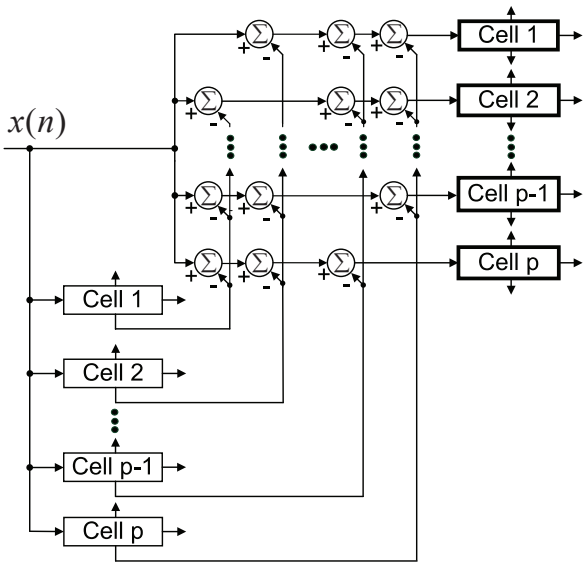

(c) The PPANFB [15].

Fig. 2 Three conventional ANFBs [4], [8], [15].

B. The Proposed ANFB

Motivated and inspired by the stated three conventional ANFBs, in this work a new ANFB, as depicted in Fig. 3, is proposed and developed that consists of a cascade form notch pre-filter bank and a parallel updated ANFB. We designate the proposed cascade and parallel ANFB as the CPANFB. The pre-filter bank is identical to the CANFB in structure except that its cells are not adapted. It is expected to preserve in part the capability of the CANFB that allows CPANFB active cells

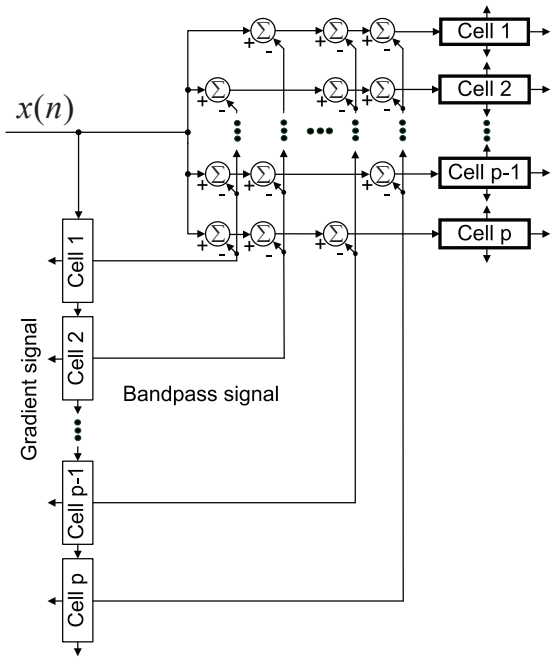

Fig. 3 Our proposed ANFB (CPANFB).

to eventually converge to different frequencies. The parallelly placed and updated cells form a simple parallel architecture of ANFB. The combination of the cascade form pre-filter bank with the parallel form ANFB allows our proposed CPANFB to enjoy the following attractive features:

1) Due to the cascade architecture of the notch pre-filter bank, the proposed CPANFB will not suffer from initialization issues that inherently and adversely impact the conventional PPANFB, even though both the CPANFB and the PPANFB have the same number of cells. This is a major advantage of our proposed CPANFB over the conventional PPANFB.
2) Even though the notch pre-filter bank in the CPANFB is of the cascade architecture rather than parallel form as adopted in the PPANFB, the SNR condition for active cells is still quite uniform as long as the notch bandwidth is set sufficiently narrow with respect to the distribution and spacing of frequencies being targeted. This feature will be further investigated and made clear in the next subsection.

Note that subsequently steady-state analysis, extensive simulation studies, and application to real noise and vibration signals will be presented to demonstrate the effectiveness and promising capabilities of our proposed CPANFB.

In the cascade architecture of the notch pre-filter bank of CPANFB, the ith cell output is given by

$$\begin{aligned} e_{c,i}(n) = & -\rho c_i(n) e_{c,i}(n-1) - \rho^2 e_{c,i}(n-2) \\ & + x(n) + c_i(n) x(n-1) + x(n-2), \ i = 1 \end{aligned} \tag{4}$$

$$\begin{aligned} e_{c,i}(n) = & -\rho c_i(n) e_{c,i}(n-1) - \rho^2 e_{c,i}(n-2) \\ & + e_{c,i-1}(n) + c_i(n) e_{c,i-1}(n-1) + e_{c,i-1}(n-2), \ i > 1. \end{aligned} \tag{5}$$

The corresponding bandpass signals are given by

$$x_{c,i}(n) = x(n) - e_{c,i}(n), \ i = 1 \tag{6}$$

$$x_{c,i}(n) = e_{c,i-1}(n) - e_{c,i}(n), \ i > 1. \tag{7}$$

The input, output and the gradient signals of the ith active cell are respectively given by

$$x_{p,i}(n) = x(n) - \sum_{j=1, j \neq i}^{p} x_{c,j}(n) \tag{8}$$

$$\begin{aligned} e_i(n) = & -\rho c_i(n) e_i(n-1) - \rho^2 e_i(n-2) \\ & + x_{p,i}(n) + c_i(n) x_{p,i}(n-1) + x_{p,i}(n-2) \end{aligned} \tag{9}$$

$$g_i(n) = x_{p,i}(n-1) - \rho e_i(n-1). \tag{10}$$

Inspired by the p-power and the MNG algorithms [13], [14], below we propose a modified NG (ModNG) scheme to update the active cells of CPANFB, as follows:

$$c_i(n+1) = c_i(n) - \mu \frac{e_i(n) g_i(n)}{\epsilon + G_i^{\gamma}(n)}, \ \gamma \geq 1 \tag{11}$$

$$G_i(n) = \alpha G_i(n-1) + (1-\alpha) g_i^2(n) \tag{12}$$

where μ denotes a small positive step size that controls the pace of algorithm convergence, ϵ denotes a small positive number that is introduced to avoid division by zero, $\alpha \in [0, 1)$ denotes a forgetting factor that is smaller than but very close to 1, γ ($\geq$ 1) is another user parameter. If γ is set to 1, the ModNG algorithm is nothing but the conventional NG algorithm. Extensive simulations conducted have shown that the ModNG significantly outperforms the conventional NG over wide range of SNR and frequency, if γ is properly selected.

The active cell (ANF) is quite sensitive to the choice of ϵ. However, ϵ can be taken between 0.001 and 0.01 to obtain acceptable and reliable results in real applications [8], [30]. The forgetting factor α does not affect the ANF significantly, as long as it is set close to 1, say 0.98, 0.99, etc. [30]. The ANF yields different performances for different values of γ. For a wide range of frequencies, putting γ to 2 yields better frequency estimation accuracy as compared to the conventional NG algorithm. Details are given in Section III. Many gradient-type algorithms for the ANF, such as the SA, PG, MNG, and their variants, among others, have been analyzed to reveal their statistical properties and to guide and facilitate the user parameter selection, refer to [6]-[19], [33] and references therein. However, the statistical analysis of NG has not yet been attempted due to the difficulty posed by lowpass filtering of the squared gradient signal in (12).

The proposed CPANFB is as efficient as the PPANFB since they both require the same number of cells [15]. The following steady-state analysis as well as extensive simulation studies will show that our CPANFB and PPANFB strategies provide quite similar frequency estimation and tracking performance if the initial cell weights are properly selected. The major advantage of our proposed CPANFB over the PPANFB is that its active cells are capable of targeting different frequencies as the adaptation process evolves irrespective of the initial filter weights setting.

C. Steady State Analysis

In this subsection, the SNR conditions and properties corresponding to active cells in steady state associated with the four ANFBs (namely, CANFB, TCANFB, PPANFB, and CPANFB) are investigated in some detail. The analysis provided here is expected to significantly enrich and deepen our understanding on the basic characteristics of ANFBs. Before considering individual ANFB, let us provide four common and insightful expressions for the amplitude and phase responses of the notch filter (2) and the corresponding bandpass filter (3) for a given frequency ω that is sufficiently apart from the notch frequency ω_0 with respect to the notch bandwidth.

The amplitude and phase responses are given below for the notch and bandpass filters, respectively. Further details are provided in the Appendices A and B.

$$A_{\rm N}(\omega,\omega_0)\approx\frac{1}{\rho}\left[1-\frac{1}{2}(1-\rho)^2\frac{1-\cos\omega\cos\omega_0}{(\cos\omega-\cos\omega_0)^2}\right] \tag{13}$$

$$\begin{aligned}\phi_{\rm N}(\omega,\omega_0)\approx&\tan^{-1}\left[-(1-\rho)\frac{\sin\omega}{\cos\omega-\cos\omega_0}\right. \\ &\left.-\frac{1}{2}(1-\rho)^2\frac{\sin\omega}{\cos\omega-\cos\omega_0}\left(2\sin^2\omega+\frac{\cos(2\omega)}{(\cos\omega-\cos\omega_0)^2}\right)\right]\end{aligned} \tag{14}$$

$$\begin{aligned}A_{\rm B}(\omega,\omega_0)\approx&(1-\rho)\sqrt{1+\left(\frac{\sin\omega}{\cos\omega-\cos\omega_0}\right)^2} \\ &+\frac{1}{2}(1-\rho)^2\frac{1}{(\cos\omega-\cos\omega_0)^2}\frac{\sin^2\omega_0-3\cos\omega_0(\cos\omega-\cos\omega_0)}{\sqrt{1+\left(\frac{\sin\omega}{\cos\omega-\cos\omega_0}\right)^2}}\end{aligned} \tag{15}$$

$$\begin{aligned}\phi_{\rm B}(\omega,\omega_0)\approx&\tan^{-1}\left[-\frac{\sin\omega}{\cos\omega-\cos\omega_0}-\frac{1}{2}(1-\rho)\left(\frac{\sin\omega}{\cos\omega-\cos\omega_0}\right.\right. \\ &\left.+\frac{\sin\omega\cos\omega}{(\cos\omega-\cos\omega_0)^2}+2\frac{\sin^3\omega}{(\cos\omega-\cos\omega_0)^3}\right) \\ &+\frac{1}{2}(1-\rho)^2\left(\frac{3\sin\omega}{\cos\omega-\cos\omega_0}+\frac{5\sin\omega\cos\omega}{2(\cos\omega-\cos\omega_0)^2}\right. \\ &+\frac{10\sin^3\omega+\sin\omega\cos^2\omega+4\sin\omega(1-\cos\omega\cos\omega_0)}{2(\cos\omega-\cos\omega_0)^3} \\ &\left.\left.+\frac{2\sin^3\omega}{(\cos\omega-\cos\omega_0)^4}+\frac{2\sin^5\omega}{(\cos\omega-\cos\omega_0)^5}\right)\right].\end{aligned} \tag{16}$$

It is commonly assumed in utilizing the ANFBs that: 1) each notch filter removes a single frequency completely while other frequencies are allowed to go through without any amplitude and phase distortions, and 2) a bandpass filter passes a given sinusoid unchanged in both amplitude and phase while other sinusoids are blocked and attenuated. The prerequisite for these attractive features to be achieved is that sinusoidal frequencies to be targeted by the ANFB must be well spaced and the notch filter bandwidth must be set adequately narrow. This has been a common empirical recognition for applying the ANFB. However, no theoretical basis has been provided yet in the literature.

From the above analytical expressions, the following insightful remarks may be concluded and established:

1) If the notch bandwidth that is proportional to $1-\rho$ is set sufficiently narrow such that $1-\rho$ is much smaller than the distance between the signal frequency ω and the notch frequency ω_0 in the form of $|\cos\omega-\cos\omega_0|$, i.e.,

$$\left|\frac{1-\rho}{\cos\omega-\cos\omega_0}\right|\ll 1 \tag{17}$$

expressions (13)-(16) may be further approximated as follows:

$$A_{\rm N}(\omega,\omega_0)\approx\frac{1}{\rho} \tag{18}$$

$$\phi_{\rm N}(\omega,\omega_0)\approx\tan^{-1}\left[-(1-\rho)\frac{\sin\omega}{\cos\omega-\cos\omega_0}\right] \tag{19}$$

$$A_{\rm B}(\omega,\omega_0)\approx(1-\rho)\sqrt{1+\left(\frac{\sin\omega}{\cos\omega-\cos\omega_0}\right)^2} \tag{20}$$

$$\begin{aligned}\phi_{\rm B}(\omega,\omega_0)\approx&\tan^{-1}\left[-\frac{\sin\omega}{\cos\omega-\cos\omega_0}\right. \\ &-\frac{1}{2}(1-\rho)\left(\frac{\sin\omega}{\cos\omega-\cos\omega_0}\right. \\ &+\frac{\sin\omega\cos\omega}{(\cos\omega-\cos\omega_0)^2} \\ &\left.\left.+2\frac{\sin^3\omega}{(\cos\omega-\cos\omega_0)^3}\right)\right]\end{aligned} \tag{21}$$

2) It follows from (18) and (19) that a sinusoid with frequency ω will pass through the notch filter having the notch frequency ω_0 and bandwidth $\pi(1-\rho)$, with its amplitude amplified by $\frac{1-\rho}{\rho}\times 100$ percent and its phase shifted by $\frac{\phi_{\rm N}(\omega,\omega_0)}{\pi}\times 180$ degrees. If the expression (17) holds the phase shift may be ignored.
3) On the other hand, a sinusoid with the frequency ω will be significantly blocked and suppressed by a bandpass filter that is derived from the notch filter, as follows from (20) and (21), with its amplitude considerably attenuated and its phase shifted by $\frac{\phi_{\rm B}(\omega,\omega_0)}{\pi}\times 180$ degrees. If the expression (17) holds the sinusoid that remains in the bandpass filter output has negligible amplitude and may be ignored in terms of its power that is proportional to $((1-\rho)/(\cos\omega-\cos\omega_0))^2$, however the phase shift still exists. Of course, the phase shift has no impact if the amplitude response is treated as zero.
4) In the CANFB, a sinusoid may be amplified many times until it is removed by the ANF. The sinusoid targeted by the last cell (Cell p) will be amplified $p-1$ times and its phase will be shifted $p-1$ times, by Cell 1, $\cdots$, to Cell $p-1$. The phase shift does not affect the CANFB performance as far as the frequency estimation is concerned.
5) In the TCANFB, any sinusoid that is targeted by an active cell will be amplified $p-1$ times, and its phase will be shifted $p-1$ times. Similar to the CANFB, the phase shift does not affect the TCANFB frequency estimation.
6) As noted from (20) and (21), no amplitude amplification occurs for any sinusoid that is targeted by an

active cell in the PPANFB, if the expression (20) is approximated by zero.

7) In our proposed CPANFB, the bandpass signals that are generated by the notch pre-filter bank cells, except for the first one that is extracted by the first cell, will all be subject to amplitude amplification and phase shift with respect to the original sinusoids. This introduces an unfavorable scenario for the CPANFB. However, this impact can be disregarded if the expression (17) is satisfied such that quantity (19) is negligible. This explains why the CPANFB is comparable or slightly inferior to the PPANFB in terms of the frequency estimation performance.

We are now in a position to analyze the SNR properties for each active cell in the four ANFBs and approximate them analytically. Without loss of generality, it is assumed that the ith active cell targets the ith frequency for $i = 1, 2, \cdots, p$ and ρ is selected to be very close to one. That is, the estimated frequency in each active cell is adequately accurate such that the filter coefficients c_i ($i = 1, 2, \cdots, p$) may be approximately set to the ideal values, namely $-2\cos\omega_i$, for sake of analysis that follows. This is an approximation that is introduced to facilitate the analysis. Nevertheless, as will be shown in the following analysis (Eqs. (25), (31), and (35)), this approximation does not cause significant errors in our analysis, due to the fact that the derived variance expressions for the additive noise involved in the input to an active cell indicate weak dependency on the filter coefficients or frequency estimates, as long as ρ is set very close to 1 and the ANFB performs as expected.

(A) The CANFB

In the input of the ith cell (with $i \geq 2$), the kth sinusoid (with $k \geq i$) satisfies the following amplitude and phase expressions:

$$\begin{aligned} A_{C,i,k} &= A_k \prod_{j=1}^{i-1} A_{\mathrm{N}}(\omega_k, \omega_j) \\ &\approx A_k \left(\frac{1}{\rho}\right)^{i-1} \end{aligned} \tag{22}$$

$$\begin{aligned} \phi_{C,i,k} &= \theta_k + \sum_{j=1}^{i-1} \phi_{\mathrm{N}}(\omega_k, \omega_j) \\ &\approx \theta_k. \end{aligned} \tag{23}$$

The variance of the additive noise $v_{C,i}(n)$ that stays in the ith cell input due to the AWGN $v(n)$ is governed by

$$\sigma^2_{C,1} = \sigma^2 \tag{24}$$

$$\begin{aligned} \sigma^2_{C,i} &= \frac{\sigma^2}{2\pi\nu} \oint_{\mathbf{c}} \prod_{m=1}^{i-1} H_{N,m}(z) H_{N,m}(z^{-1}) \frac{dz}{z}, \nu = \sqrt{-1}, i > 1 \\ &= \sigma^2 \left\{ \frac{1}{\rho^{2(i-1)}} + \frac{1-\rho}{1+\rho} \sum_{m=1}^{i-1} [f_C(z_{m,1}, z_{m,2}) + f_C(z_{m,2}, z_{m,1})] \right\} \\ &\approx \left[\frac{1}{\rho^2} \left(1 - 2\frac{1-\rho}{1+\rho} \right) \right]^{i-1} \sigma^2 \end{aligned} \tag{25}$$

where $H_{N,m}(z)$ denotes the transfer function of the notch filter (2) with the filter coefficient c_m $(= -2\cos\omega_m)$,

$$\begin{aligned} f_C(z_{m,1}, z_{m,2}) &= \frac{(c_m z_{m,1} + 1 + \rho)^2}{z_{m,1}(z_{m,1} - z_{m,2})(1 - z^2_{m,1})} \\ &\times \prod_{k=1, k\neq m}^{i-1} \frac{z^2_{m,1} + c_k z_{m,1} + 1}{(z_{m,1} - z_{k,1})(z_{m,1} - z_{k,2})} \frac{1 + c_k z_{m,1} + z^2_{m,1}}{1 + \rho c_k z_{m,1} + \rho^2 z^2_{m,1}} \end{aligned} \tag{26}$$

$$z_{m,1} = \rho e^{\nu\omega_m},\ z_{m,2} = \rho e^{-\nu\omega_m},\ m = 1, 2, \cdots, p. \tag{27}$$

and $\mathbf{c}$ denotes a unit circle centered at origin in the z-domain. Note that the residues theory is applied in the derivations of (25). Further details are provided in the Appendix C.

The SNR for the first, the kth and the last cell, where $1 < k < p$ are respectively computed as

$$\mathrm{SNR}_{C,1} = 10\log 10 \left(\frac{A_1^2/2}{\sigma^2 + \sum_{k=2}^{p} A_k^2/2} \right) \tag{28}$$

$$\begin{aligned} \mathrm{SNR}_{C,k} &= 10\log 10 \left(\frac{A_k^2/(2\rho^{2(k-1)})}{\sigma^2_{C,k} + \sum_{m=k+1}^{p} A_m^2/(2\rho^{2(k-1)})} \right) \\ &= 10\log 10 \left(\frac{A_k^2/2}{\left(1 - 2\frac{1-\rho}{1+\rho}\right)^{k-1} \sigma^2 + \sum_{m=k+1}^{p} A_m^2/2} \right) \\ &\approx 10\log 10 \left(\frac{A_k^2/2}{\rho^{k-1}\sigma^2 + \sum_{m=k+1}^{p} A_m^2/2} \right) \end{aligned} \tag{29}$$

$$\begin{aligned} \mathrm{SNR}_{C,p} &= 10\log 10 \left(\frac{A_p^2/(2\rho^{2(p-1)})}{\sigma^2_{C,p}} \right) \\ &\approx 10\log 10 \left(\frac{A_p^2/2}{\rho^{p-1}\sigma^2} \right). \end{aligned} \tag{30}$$

(B) The TCANFB

The variance of additive noise in the input of the kth active cell may be computed following along similar lines as that in (25) to obtain

$$\begin{aligned} \sigma^2_{TC,k} &= \frac{\sigma^2}{2\pi\nu} \oint_{\mathbf{c}} \prod_{m=1, m\neq k}^{p} H_{N,m}(z) H_{N,m}(z^{-1}) \frac{dz}{z} \\ &\approx \left[\frac{1}{\rho^2} \left(1 - 2\frac{1-\rho}{1+\rho} \right) \right]^{p-1} \sigma^2 \end{aligned} \tag{31}$$

which clearly is not related to k, implying that all the active cells in the TCANFB are equally and uniformly disturbed by the additive noise due to $v(n)$.

The SNR of the kth active cell in the TCANFB may be given by

$$\begin{aligned}\mathrm{SNR}_{TC,k} &= 10\log10\left(\frac{A_k/(2\rho^{2(p-1)})}{\sigma^2_{TC,k}}\right) \\ &\approx 10\log10\left(\frac{A_k/2}{\rho^{p-1}\sigma^2}\right).\end{aligned} \tag{32}$$

(C) The PPANFB

Here, $v_{b,i}(n)$ and $v_{p,i}(n)$ are used to denote the additive noise in the output signal of the ith bandpass pre-filter and the input signal of the ith active cell, respectively,

$$v_{p,i}(n) = v(n) - \sum_{m=1,m\neq i}^{p} v_{b,m}(n). \tag{33}$$

The variance of $v_{p,i}(n)$ may be obtained as

$$\begin{aligned}E[v^2_{p,i}(n)] &= \sigma^2 + \sum_{m=1,m\neq i}^{p} E[v^2_{b,m}(n)] \\ &+ \sum_{m_1=1,m_1\neq i}^{p} \sum_{m_2=1,m_2\neq i,m_2\neq m_1}^{p} E[v_{b,m_1}(n)v_{b,m_2}(n)]\end{aligned} \tag{34}$$

where $E[v(n)v_{b,m}(n)] = 0$, is used in obtaining the above equation for any m. The variance of $v_{b,m}(n)$ is expressed by

$$\begin{aligned}E[v^2_{b,m}(n)] &= (1-\rho)\sigma^2\left\{\frac{2}{1+\rho}+\frac{2(1-\rho)^2(2+\rho)}{(1+\rho)(\rho^4-2\rho^2\cos(2\omega_m)+1)}\right. \\ &\left. -\frac{(1-\rho)^2\left[(1+\rho)^2+4\sin^2\omega_m\right]}{(1+\rho)(\rho^4-2\rho^2\cos(2\omega_m)+1)}\right\} \\ &\approx \frac{2(1-\rho)}{1+\rho}\sigma^2.\end{aligned} \tag{35}$$

The derivation of (35) is given in [34]. The correlation between $v_{b,m_1}(n)$ and $v_{b,m_2}(n)$ for $m_1 \neq m_2$ is given as follows:

$$\begin{aligned}&E[v_{b,m_1}(n)v_{b,m_2}(n)] \\ &= \frac{(1-\rho)^2\sigma^2}{2\pi\nu}\oint_{\mathbf{c}} \frac{c_{m_1}z+1+\rho}{z^2+\rho c_{m_1}z+\rho^2}\frac{c_{m_2}+(1+\rho)z}{1+\rho c_{m_2}z+\rho^2 z^2}dz \\ &= (1-\rho)^2\sigma^2\left[f_P(m_1,m_2,z_{m_1},z_{m_2})\right. \\ &\quad \left.+f_P(m_1,m_2,z_{m_2},z_{m_1})\right] \\ &f_P(m_1,m_2,z_1,z_2) = \frac{(c_{m_1}z_1+1+\rho)[c_{m_2}+(1+\rho)z_1]}{(z_1-z_2)(1+\rho c_{m_2}z_1+\rho^2 z_1^2)}.\end{aligned} \tag{36, 37}$$

Clearly, $E[v_{b,m_1}(n)v_{b,m_2}(n)]$ can be set to zero as compared to $E[v^2_{b,m}(n)]$. Therefore, the SNR of the kth active cell in the PPANFB may be approximated by

$$\mathrm{SNR}_{PP,k} = 10\log10\left(\frac{A_k^2/2}{\sigma^2+2\frac{(1-\rho)}{1+\rho}(p-1)\sigma^2}\right). \tag{38}$$

(D) The proposed CPANFB

Here, $v_{x_b,i}(n)$ and $v_{x_p,i}(n)$ are used to denote the additive noise in the output signal of the ith bandpass pre-filter and the input signal of the ith active cell, respectively. Following the results and approximations provided in the Appendix C, we obtain

$$E[v^2_{x_b,1}(n)] \approx \frac{2(1-\rho)}{1+\rho}\sigma^2 \tag{39}$$

$$E[v^2_{x_b,m}(n)] \approx \frac{2(1-\rho)}{1+\rho}\left[\frac{1}{\rho^2}\left(1-2\frac{1-\rho}{1+\rho}\right)\right]^{m-1}\sigma^2,\ 2\leq m\leq p. \tag{40}$$

The correlation between $v_{x_b,m_1}(n)$ and $v_{x_b,m_2}(n)$ for $m_1 \neq m_2$ may be ignored as it is proportional to $(1-\rho)^2$. The additive noise $v_{x_p,i}(n)$ is given by

$$v_{x_p,i}(n) = v(n) - \sum_{m=1,m\neq i}^{p} v_{x_b,m}(n) \tag{41}$$

whose variance may be obtained as

$$\begin{aligned}E[v^2_{x_p,i}(n)] &= \sigma^2 + \sum_{m=1,m\neq i}^{p} E[v^2_{x_b,m}(n)] \\ &+ \sum_{\substack{m_1=1,\\ m_1\neq i}}^{p}\sum_{\substack{m_2=1,\\ m_2\neq i,\\ m_2\neq m_1}}^{p} E[v_{x_b,m_1}(n)v_{x_b,m_2}(n)] \\ &\approx \sigma^2 + \sum_{m=1,m\neq i}^{p} E[v^2_{x_b,m}(n)] \\ &\approx \sigma^2 + \frac{2(1-\rho)}{1+\rho}\sigma^2\sum_{\substack{m=1,\\ m\neq i}}^{p}\left[\frac{1}{\rho^2}\left(1-2\frac{1-\rho}{1+\rho}\right)\right]^{m-1}.\end{aligned} \tag{42}$$

Consequently, the SNR for the kth active cell in the CPANFB may be approximated by

$$\mathrm{SNR}_{CP,k} = 10\log10\left(\frac{A_k^2/2}{\sigma^2+\frac{2(1-\rho)}{1+\rho}\sigma^2\sum\limits_{\substack{m=1,\\ m\neq k}}^{p}\left[\frac{1}{\rho^2}\left(1-2\frac{1-\rho}{1+\rho}\right)\right]^{m-1}}\right). \tag{43}$$

The following observations may be drawn from the analytical expressions (22)-(43).

8) From the expressions (28)-(30), it follows that the SNR for the CANFB cell improves as the cell number changes from 1 to p, with the first cell having the poorest and the last cell enjoying the best operating condition.
9) The SNRs for the active cells in TCANFB, PPANFB, and CPANFB are almost uniform, as seen from (32), (38), and (43).
10) The SNR given in (32) and (30) for every TCANFB and the last CANFB active cell respectively is the largest as compared to those of the other two ANFBs (i.e., PPANFB, CPANFB). It may become very close to the best achievable SNR value, i.e., $10\log10(A_k^2/(2\sigma^2))$.
11) The SNRs of active cells in PPANFB and CPANFB, provided in (38) and (43), are smaller than that of the

TCANFB given by (32), implying that the TCANFB is the best ANFB in terms of the active cell input SNR.

12) Given that

$$\left(1-2\frac{1-\rho}{1+\rho}\right)-\rho^2$$

is slightly larger than zero, then it follows that

$$\sum_{m=1,m\neq k}^{p}\left[\frac{1}{\rho^2}\left(1-2\frac{1-\rho}{1+\rho}\right)\right]^{m-1}$$

is slightly larger than $p-1$, and the SNR of CPANFB in (43) will be slightly smaller than that of the PPANFB in (38). That is to say, the CPANFB may be comparable or slightly inferior to the PPCANFB as far as the frequency estimation is concerned, as will be shown in next section. However, the CPANFB yields results that are much less sensitive to the initial filter weight setting that would otherwise severely damage the PPANFB results in real applications.

III. Simulations and Comparative Case Studies

Extensive simulations and comparative case studies are now performed to verify and validate the effectiveness and capabilities of the improved performance of our proposed CPANFB equipped with the ModNG algorithm. Three groups of representative simulation results are provided below.

A. Influence of the Initial Filter Weight Selection

To compare our proposed CPANFB and its counterpart PPANFB in terms of the initial weight setting, we simulated a case with three noisy sinusoids that have uniform energy ($A_i = 1, i = 1, 2, 3$). Frequencies of the sinusoids are 0.2π, 0.4π and 0.6π. The SNR for each sinusoid is 1 [dB].

The simulation results are provided in Fig. 4, where two initial filter weight settings are tested. In the first setting, all the filter weights are set to zero. This setting indicates a situation where limited or no information on the signal frequency distribution is available in advance. As shown in Fig. 4(a), every cell in the CPANFB gradually targets one of the three frequencies as the adaptation process evolves. However, all the PPANFB cells eventually converge to the same frequency, rendering the PPANFB powerless in identifying the three frequencies. The second setting results are presented in Fig. 4(b), where the initial weights correspond to frequencies 0.1π, 0.3π, and 0.5π which are located in the neighborhood of the true frequencies. Obviously, again, our CPANFB successfully targets all the frequencies, whereas the two active cells of the PPANFB eventually get together and are caught in the vicinity of one of the three frequencies after trying to search for different frequencies. From these two typical sets of simulation results, one can conclude that if the initial filter weights are not properly set, the PPANFB will lose its capability, whereas the CPANFB is basically not affected by the initial filter weight setting.

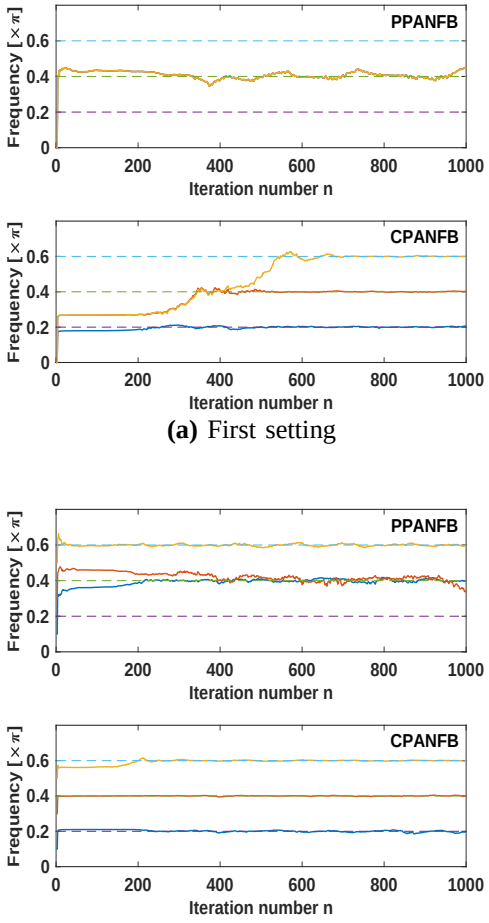

(a) First setting

(b) Second setting

Fig. 4 Convergence behavior of PPANFB and CPANFB for different initial filter weight settings (dashed line: true frequency, solid line: estimated frequency, $\omega_1 = 0.2\pi$, $\omega_2 = 0.4\pi$, $\omega_3 = 0.6\pi$, SNR=1[dB], $\rho = 0.97$, $\epsilon = 0.01$, $\alpha = 0.98$, $\gamma = 2$, $\mu = 0.005$ (PPANFB), $\mu = 0.001$ (CPANFB)). (a) $c_i(1) = 0, i = 1, 2, 3$. (b) $c_1(1) = -2\cos(0.10\pi)$, $c_2(1) = -2\cos(0.30\pi)$, $c_3(1) = -2\cos(0.50\pi)$.

B. Performance of the ModNG Algorithm

The ModNG algorithm is also proposed in this work. Here, comparisons between the conventional NG and the ModNG algorithms are presented to demonstrate that the ModNG algorithm enjoys improved performance as compared to the NG algorithm over wide ranges of signal frequency and SNR. The step size of the ModNG is adjusted for a given NG step size such that both algorithms converge in quite the same pace in terms of the estimation MSE or present similar steady-state estimation MSE. Consequently, through this mechanism fair comparisons between both algorithms may be made based on their steady-state estimation MSE or convergence rates. In all comparisons shown in Fig. 5, the MSEs are averaged over 300 independent Monte Carlo runs.

Fig. 5(a) depicts a comparison on convergence rates between the two algorithms that yielded quite similar steady-state

MSEs. Clearly, the ModNG algorithm converges much faster than the NG algorithm for the same steady-state estimation accuracy. In Fig. 5(b) and Fig. 5(c), comparisons are made in terms of the steady-state MSE that are generated by both algorithms for different signal frequency and SNR values, respectively. It follows from the results shown that the ModNG algorithm outperforms the NG algorithm over wide frequency and SNR ranges. Furthermore, the parameter γ in the ModNG algorithm was carefully investigated to reveal its effect to the steady-state MSE of the algorithm. Fig. 5(d) illustrates the variation of the MSE with respect to γ for three different signal frequencies. In this subfigure, the MSE values at $\gamma = 0$ are obtained by using the PG algorithm having a step size $\mu/(\epsilon + 1)$. Similarly, the points at $\gamma = 1$ indicate the MSEs using the NG algorithm. The MSEs at $\gamma = 2$ are the minimum points for each of the three plots, implying that the proposed ModNG algorithm yields its best performance if γ is set to 2.

Therefore, one may conclude that the ModNG algorithm provides significant performance improvement as compared to the conventional NG algorithm over wide SNR and frequency ranges, if γ is properly selected. However, as seen from Fig. 5(b), our ModNG algorithm performs poorly as compared to the conventional NG algorithm in the close neighborhood of 0.1π, 0.5π, and 0.9π. Unfortunately, at this time no analytical or intuitive explanations to this deficiency is available. Statistical analysis of our proposed ModNG and the conventional NG algorithms has not yet been attempted, due to the fact that the lowpass filtering update in (12) poses analytical difficulties. In-depth analysis of both algorithms is a technically demanding topic for our future research.

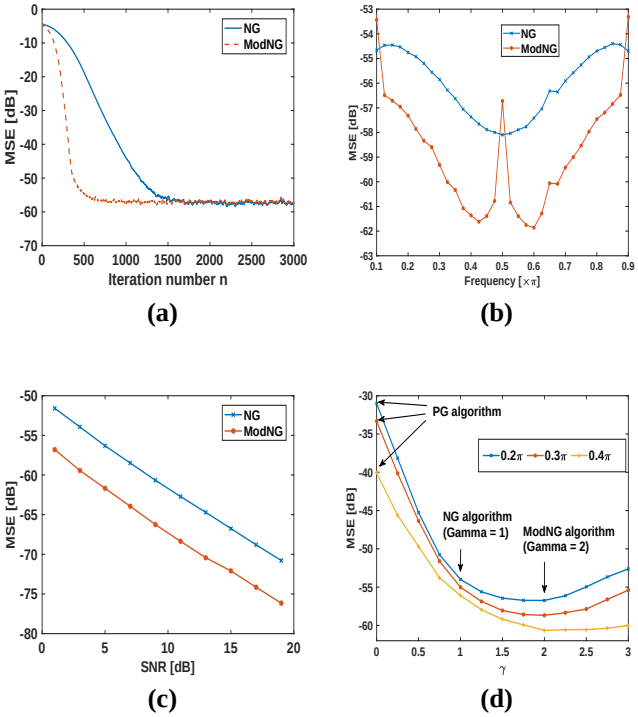

Fig. 5 Comparisons between the NG and the ModNG algorithms ($\rho = 0.95$, $\alpha = 0.98$, $\epsilon = 0.01$, 300 runs).
(a) Convergence rates of the NG and the ModNG for the same steady-state MSE ($\omega = 0.4\pi$, SNR = 3 [dB], $\mu = 0.0008$ (NG), $\mu = 0.00028$ (ModNG), $\gamma = 2$ (ModNG)).
(b) Steady-state MSE of the NG and the ModNG versus the signal frequency for a fixed convergence rate (SNR = 3 [dB], $\mu = 0.0005$ (NG), $\gamma = 2$ (ModNG)).
(c) Steady-state MSE of the NG and the ModNG versus the SNR for a fixed convergence rate ($\omega = 0.6\pi$, $\mu = 0.0005$ (NG), $\gamma = 2$ (ModNG)).
(d) Steady-state MSE of the ModNG versus γ for a fixed convergence rate (SNR = 3 [dB], $\mu = 0.0006$ (NG)).

C. *Performance of the PPANFB and CPANFB*

For a detailed performance comparison between the CPANFB and PPANFB, steady state estimation statistics (bias, standard deviations, and MSE) are provided below. Three ANFBs are considered, namely, the NG-based PPANFB, the NG-based CPANFB, and the ModNG-based CPANFB. They are abbreviated as M1, M2 and M3, respectively. Signal frequencies are 0.25π, 0.35π, and 0.45π. The ANFB initial filter weights are set to $-2\cos(0.20\pi)$, $-2\cos(0.30\pi)$ and $-2\cos(0.40\pi)$, to ensure that all the ANFBs present high probability of convergence under different SNR conditions. All the sinusoids have the same power. The pole radius ρ and the step size of M1 are fixed at 0.975 and 0.00025, respectively. User parameter γ was set to 2 in M3. The step sizes of M2 and M3 are carefully adjusted such that the three ANFBs indicate quite similar convergence and the obtained steady state statistics serve the comparison purpose quite well. Table 1 summarizes the steady state estimation bias, standard deviation and MSE of the three ANFBs for different SNR values. Three hundred (300) independent Monte Carlo runs are conducted to increase our confidence on the statistics results that are given in Table 1.

As shown in Table 1, our proposed CPANFB that is equipped with the NG algorithm is comparable or slightly inferior to the NG-based PPANFB. This observation is consistent with the analysis that was provided in Section 2. However, our CPANFB that utilizes the ModNG algorithm significantly outperforms the other two ANFBs in terms of the standard deviation and MSE.

IV. Application to Real Signals

In this section, our goal is to apply our proposed CPANFB to real noise and vibration signals to further verify, validate, and illustrate its effectiveness and confirm and demonstrate its applicability. The outcome of the CPANFB is expected to be used and served for the purposes of monitoring, maintenance decision making, fault detection and diagnosis, noise/vibration countermeasure, among others. Specifically, application to three different real signals are considered.

A. *A Noise Signal Generated by a Cutting Machine*

The first actual signal is a noise that was generated by a large-scale factory cutting machine called stand-cutter. The cutting machine was running at a rotational speed of 1600

TABLE I: Steady state performance comparison of three ANFBs.

SNR [dB]	ω/π	Bias $\times 10^{-5}$			Std $\times 10^{-4}$			MSE $\times 10^{-8}$		
		M1	M2	M3	M1	M2	M3	M1	M2	M3
1	0.25	22.423	30.592	5.027	4.014	4.182	2.638	218.484	276.712	85.573
	0.35	13.332	18.072	5.455	3.290	3.361	2.012	131.402	151.445	49.929
	0.45	7.744	8.348	4.433	2.984	2.983	1.698	100.010	100.925	36.115
5	0.25	8.889	12.002	1.671	2.471	2.560	1.488	70.301	81.420	24.197
	0.35	5.145	7.217	2.074	1.966	2.004	1.117	42.298	46.425	13.873
	0.45	2.806	3.369	1.563	1.796	1.794	0.951	33.912	34.172	10.062
10	0.25	3.347	4.325	0.982	1.376	1.424	0.847	20.316	22.417	7.498
	0.35	1.660	2.611	0.928	1.085	1.107	0.632	12.199	13.106	4.198
	0.45	0.451	0.990	0.464	0.986	0.982	0.537	9.895	9.893	2.991
15	0.25	1.599	1.928	0.854	0.777	0.805	0.505	6.353	6.910	2.667
	0.35	0.628	1.239	0.699	0.609	0.625	0.376	3.787	4.093	1.482
	0.45	-0.202	0.329	0.147	0.558	0.551	0.318	3.154	3.083	1.030
20	0.25	1.089	1.215	0.835	0.450	0.466	0.291	2.161	2.341	0.926
	0.35	0.274	0.778	0.583	0.341	0.356	0.214	1.183	1.341	0.496
	0.45	-0.430	0.097	0.007	0.323	0.311	0.178	1.074	0.978	0.322

M1: NG-based PPANFB, M2: NG-based CPANFB, and M3: ModNG-based CPANFB.

rpm and 1400 rpm in the first and second halves, respectively. The noise can be modeled as a sinusoidal signal with noise [35]. The original sampling frequency is 10.24 kHz. Since the noise signal presents its energy in the low-frequency range, a digital linear phase FIR low-pass filter with a length of 81 and a cutoff frequency of 2500 Hz was applied to the raw signal data. The resulting noise signal is then fed to the ANFBs, with its spectrum being depicted in Fig. 6.

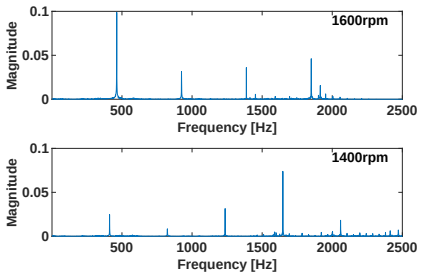

Fig. 6 Spectrum of a real noise signal generated by a cutting machine (strandcutter) (top: 1st half, 1600 rpm, bottom: 2nd half, 1400 rpm).

It follows from the spectrum depicted in Fig. 6 (top) that five prominent frequency components exist in the first half, with four being strong and one being weak. Similarly, five frequency components are present in the second half, with three being strong and two being weak. It also follows that all the target components are in the low-frequency range. Therefore, the initial weights are all set to -2 such that the ANFB can start to search and target the low frequencies in early stages of the adaptation process. Simulations illustrate that this strategy leads to better convergence performance.

Generally, the number of active cells in the ANFB needs to be set larger than that of the target frequencies. Here, six active cells are included. The frequency tracking results are shown in Fig. 7, where the solid lines represent the frequency estimates that are provided by the ANFB active cells. The broken and dash-dotted lines indicate the target frequencies for the 1^{st} and 2^{nd} halves, respectively. For sake of comparison the results of the PPANFB are included in Fig. 7(b). Fig. 7(a) shows clearly that our proposed CPANFB is capable of effectively tracking frequency components even including the weak ones. Due to the cascade-form notch pre-filter bank, frequency estimates of the CPANFB do not overlap with each other. As the adaptation process of the CPANFB approaches its steady state, the target frequencies are correctly identified and closely tracked by active cells, with the remaining active cell(s) competing against nearby active cell(s).

On the other hand, as shown in Fig. 7(b), the PPANFB has started from where the CPANFB was, however it could not identify the five target frequencies, with all active cells converging to the same target frequency, rendering the solution incomplete. A suitable initialization point can be determined for the PPANFB based on a linear relationship that can be established between the noise fundamental frequency and the rotational speed at the expense of placing an additional tachometer [35]. Clearly, additional cost is involved and technical issues must also be considered such as how to reset the PPANFB filter weights if the rotational speed is continuously time-varying, how to deal with the inaccuracy of the rotational speed measurement called the frequency mismatch [35], among others.

B. A Real Noise Generated by a Large Scale Extruder

The second real signal considered is a noise that was generated by a large-scale extruder. The extruder was running at a speed of 300 rpm and 600 rpm in the first and second half of measurements, respectively. The original sampling rate is 48 kHz. Again, a digital linear phase FIR low-pass filter with a length of 81 and a cutoff frequency of 2500 Hz was first used to filter the raw signal. The filtered noise was then decimated by a factor of 5, leading to a sampling frequency of 9600 Hz. Here, down sampling was done to project the low frequencies into a range between 0.1π and 0.9π to allow the ANFB to target and track more effectively. This is due to the fact that the second-order IIR notch filters (active cells) tend to present poor detecting capabilities and slow convergence rates if the

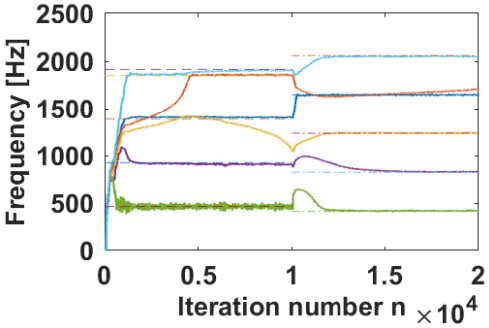

(a) The CPANFB.

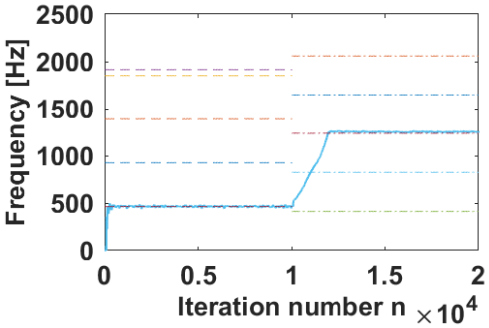

(b) The PPANFB.

Fig. 7 Frequency tracking results (dashed line: real frequency (1st half), dotted-dashed line: real frequency (2nd half), solid line: estimated frequency, $\rho = 0.95$, $\epsilon = 0.01$, $\alpha = 0.98$). (a) The CPANFB ($\mu = 0.012$, $\gamma = 1$), and (b) The PPANFB ($\mu = 0.0025$).

target frequency is smaller than 0.1π or larger than 0.9π [13]-[19], [33]. However, down sampling may adversely impact the ANFB tracking rate. In real applications, a tradeoff is required between the tracking speed and the detecting performance. The resulting noise spectrum is depicted in Fig. 8.

The noise signal in the first half contains a single dominate frequency component, whereas three prominent frequencies are included in the second half, as shown in Fig. 8. To ensure that every frequency can be targeted and tracked, four active cells were placed in the CPANFB. Similarly, we set the initial filter weights all to -2 so that the frequency targeting starts from the low-frequency range.

The frequency tracking results are illustrated in Fig. 9, where the solid lines represent the frequency estimates targeted and tracked by the active cells, and the broken and the dash-dotted lines indicate the target frequencies. As expected, in Fig. 9, the dominate frequencies over the entire adaptation duration are correctly localized and steadily tracked by our proposed CPANFB. Interestingly, a frequency around 1800 Hz only appears in the second half, and an active cell successfully targeted and estimated it very quickly. This implies that the proposed CPANFB does enjoy promising capabilities in targeting and tracking multiple frequencies in presence of additive noise.

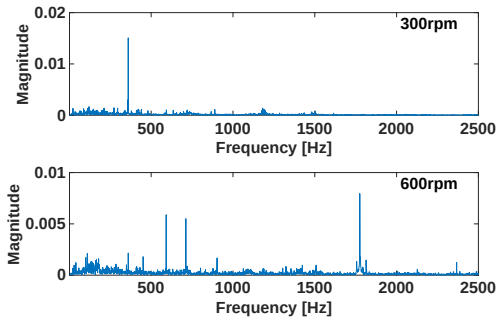

Fig. 8 Spectrum of a real noise signal generated by an extruder (top: 1st half, 300 rpm, bottom: 2nd half, 600 rpm).

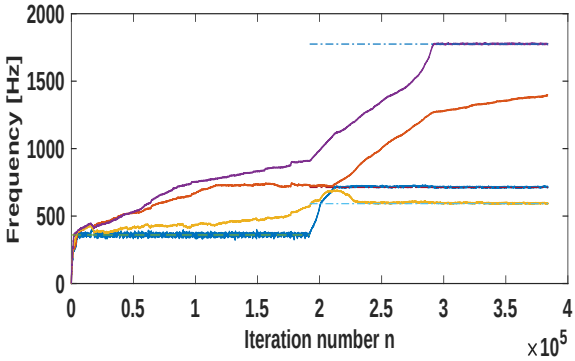

Fig. 9 Frequency tracking results obtained by utilizing our proposed CPANFB (dashed line: real frequency (1st half), dotted-dashed line: real frequency (2nd half), solid line: estimated frequency, $\rho = 0.978$, $\epsilon = 0.01$, $\alpha = 0.98$, $\mu = 0.022$, $\gamma = 2$).

C. A Vibration Signal Generated by a High Speed Train

In the above two subsections, our proposed CPANFB was demonstrated to be effective in extracting main frequency components that are included in real noise signals. Now, we show the application of the CPANFB to a real vibration signal that was generated by a high-speed train that is owned by the Chinese Railway.

The cardan shaft is a core part of a high-speed train transmission system, and detection of its dynamic imbalance is of great significance in ensuring safety of the train operation [36]. The dynamic imbalance features of the cardan shaft are manifested as characteristic (fault) frequency in the vibration signal spectrum. This signal (rail-measured acceleration time sequence) was measured on a motor. The sampling frequency is 10 kHz. The train was running at the speed of 200 Km/h. Since the fault frequency and its harmonics are located in the low-frequency range, the raw vibration signal was first fed to a digital linear phase FIR low-pass filter with a length of 81 and the cutoff frequency of 300 Hz. The low-pass filtered signal was then decimated by a factor of 20 before it was applied to the CPANFB. The resultant sampling frequency f_s is equal

to 500 Hz. The spectrum of the resulting vibrational signal is presented in Fig. 10, which bears a dynamic imbalance fault with the cardan shaft.

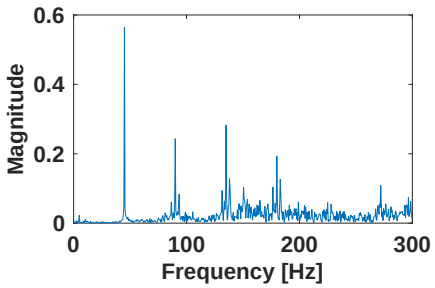

Fig. 10 Spectrum of a real vibrational signal generated by a high-speed train.

The frequency tracking results obtained from the CPANFB are shown in Fig. 11. Clearly, the rotational frequency and the first two harmonics are clearly targeted and tracked. Estimation of the last harmonic frequency indicates relatively large fluctuations due to its low amplitude and the nearby significant disturbances. One of the active cells is alternating between two target frequencies that are being tracked by the other two active cells.

Admittedly, from a practical point of view, an approximate range of the fault frequency can be estimated from experience with the dynamic imbalance faults. The fault frequency usually lies in a range from 34Hz to 56 Hz. Therefore, we may obtain reasonable initial filter weights in advance for the ANFB. In this simulation, we also intentionally adopted a set of initial filter weights that were put to $-2\cos(i\omega_0)$ ($\omega_0 = 2\pi f_0/f_s$, $f_0 = 30$ Hz, $f_s = 500$ Hz, $i = 1, 2, \cdots, 5$), with all active cells starting from the close neighborhood of the fault frequency ($f_0 = 30$ Hz) and its harmonics (60 Hz, 90 Hz, 120 Hz, and 150 Hz).

The tracking results are shown in Fig. 12. With utilization of suitable initial filter weights, as seen in Fig. 12(a), each active cell in our proposed CPANFB finds a different target frequency more quickly. However, as noted in Fig. 12(b), four active cells of the PPANFB eventually targeted the same frequency, with the last weak harmonic unattended and undetected. Fig. 12 reveals that there is a high probability that multiple active cells in the PPANFB may target the same frequency even when a reasonable set of initial filter weights are set based on knowledge and experience regarding the object that generates the signal. On the contrary, our proposed CPANFB hardly suffers from the filter weight initialization problem and is thus more suitable for real-life applications.

To summarize, our proposed CPANFB enjoys higher applicability to actual and real noise and vibrational signals as compared to the conventional PPANFB.

V. Conclusions

In this paper, we can summarize our three major contributions as follows:

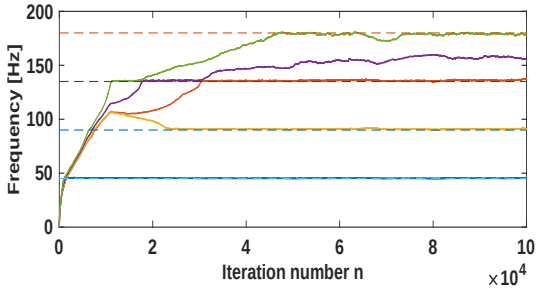

Fig. 11 Frequency tracking results obtained by utilizing the CPANFB (dashed line: real frequency, solid line: estimated frequency, $\rho = 0.96$, $\epsilon = 0.01$, $\alpha = 0.98$, $\gamma = 2$, $\mu = 0.0009$).

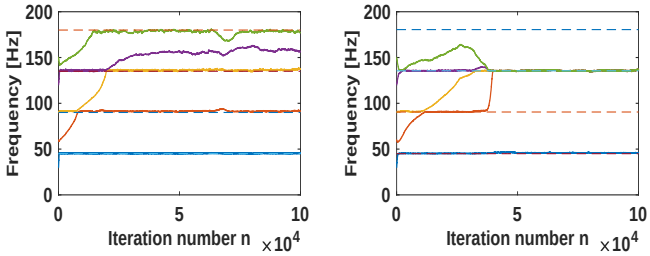

(a) The CPANFB. **(b)** The PPANFB.

Fig. 12 Frequency tracking results (dashed line: real frequency, solid line: estimated frequency, $\rho = 0.96$, $\epsilon = 0.01$, $\alpha = 0.98$). (a) The CPANFB ($\mu = 0.0001$, $\gamma = 2$). (b) The PPANFB ($\mu = 0.0006$).

1) A novel ANFB is proposed that has an architecture consisting of both a cascade notch pre-filter bank and a parallel one. The filter weight initialization challenge that is prevailing in the conventional PPANFB in the literature is significantly alleviated by our proposed ANFB.
2) A modified version of the NG algorithm has been proposed that works significantly better than the conventional NG algorithm over wide ranges of frequency and SNR.
3) Formal steady-state analysis is conducted in detail corresponding to four ANFBs including our proposed CPANFB and SNR for active cells is provided through insightful and closed-form expressions, which significantly enhances our understanding of the ANFBs.

Furthermore, extensive simulations as well as applications to three real-life noise and vibrational signals have been performed to demonstrate the effectiveness and superiority of our proposed CPANFB over its counterpart PPANFB. Future research topics include challenges related to: 1) modification of the CPANFB structure, 2) in-depth statistical analysis of the ModNG algorithm and the CPANFB, and 3) fault detection and diagnosis based on the use of ANFBs.

Appendix A: Notch filter frequency response

If the input to the IIR notch filter as given by (2) with the notch frequency ω_0 contains a sinusoid whose frequency ω is identical or very close to the notch frequency ω_0, the sinusoid will be attenuated and reduced to a negligible level in the filter output. What will happen if ω is quite far away from the notch frequency ω_0? To get an insightful answer, we need to investigate the frequency response of the IIR notch filter in a particular manner.

The amplitude response of (2) may be expressed as

$$A_{\mathrm{N}}(\omega,\omega_0)=|H_{\mathrm{N}}(e^{\nu\omega})| =\frac{1}{\rho}f_{\mathrm{N}}(\rho,\omega,\omega_0) \tag{44}$$

$$f_{\mathrm{N}}(\rho,\omega,\omega_0)=\frac{1}{\sqrt{\left[\frac{1-2\rho\cos\omega_0\cos\omega+\rho^2\cos(2\omega)}{2\rho(\cos\omega-\cos\omega_0)}\right]^2+\left[\frac{\sin\omega(\cos\omega_0-\rho\cos\omega)}{\cos\omega-\cos\omega_0}\right]^2}}.$$

Now if one applies the Taylor series expansion to $f_{\mathrm{N}}(\rho,\omega,\omega_0)$ with respect to ρ in the vicinity of one, we gets

$$f_{\mathrm{N}}(\rho,\omega,\omega_0)=f_{\mathrm{N}}(\rho,\omega,\omega_0)|_{\rho=1}-(1-\rho)\frac{\partial f_{\mathrm{N}}(\rho,\omega,\omega_0)}{\partial\rho}|_{\rho=1} +\frac{1}{2}(1-\rho)^2\frac{\partial^2 f_{\mathrm{N}}(\rho,\omega,\omega_0)}{\partial\rho^2}|_{\rho=1}+\cdots. \tag{45}$$

After some lengthy derivations, one gets

$$f_{\mathrm{N}}(\rho,\omega,\omega_0)|_{\rho=1} = 1 \tag{46}$$

$$\frac{\partial f_{\mathrm{N}}(\rho,\omega,\omega_0)}{\partial\rho}|_{\rho=1} = 0 \tag{47}$$

$$\frac{\partial^2 f_{\mathrm{N}}(\rho,\omega,\omega_0)}{\partial\rho^2}|_{\rho=1} = -\frac{1-\cos\omega\cos\omega_0}{(\cos\omega-\cos\omega_0)^2}. \tag{48}$$

Putting (45)-(48) into (44) and truncating terms with orders higher than 3 leads to (13). The phase response is given by

$$\phi_{\mathrm{N}}(\rho,\omega,\omega_0)=\tan^{-1}Q_{\mathrm{N}}(\rho,\omega,\omega_0) \tag{49}$$

$$Q_{\mathrm{N}}(\rho,\omega,\omega_0)=\frac{Q_{N_b}(\omega,\omega_0)Q_{N_c}(\rho,\omega,\omega_0)-Q_{N_a}(\omega,\omega_0)Q_{N_d}(\rho,\omega,\omega_0)}{Q_{N_a}(\omega,\omega_0)Q_{N_c}(\rho,\omega,\omega_0)+Q_{N_b}(\omega,\omega_0)Q_{N_d}(\rho,\omega,\omega_0)} \tag{50}$$

$$Q_{N_a}(\omega,\omega_0)=1-2\cos\omega_0\cos\omega+\cos(2\omega) \tag{51}$$

$$Q_{N_b}(\omega,\omega_0)=2\cos\omega_0\sin\omega-\sin(2\omega) \tag{52}$$

$$Q_{N_c}(\rho,\omega,\omega_0)=1-2\rho\cos\omega_0\cos\omega+\rho^2\cos(2\omega) \tag{53}$$

$$Q_{N_d}(\rho,\omega,\omega_0)=2\rho\cos\omega_0\sin\omega-\rho^2\sin(2\omega). \tag{54}$$

Similarly, $Q_{\mathrm{N}}(\rho,\omega,\omega_0)$ may be expressed as given below by virtue of the Taylor series expansion with respect to ρ in the vicinity of one as follows

$$Q_{\mathrm{N}}(\rho,\omega,\omega_0)=Q_{\mathrm{N}}(\rho,\omega,\omega_0)|_{\rho=1}-(1-\rho)\frac{\partial Q_{\mathrm{N}}(\rho,\omega,\omega_0)}{\partial\rho}|_{\rho=1} +\frac{1}{2}(1-\rho)^2\frac{\partial^2 Q_{\mathrm{N}}(\rho,\omega,\omega_0)}{\partial\rho^2}|_{\rho=1}+\cdots. \tag{55}$$

Substituting

$$Q_{\mathrm{N}}(\rho,\omega,\omega_0)|_{\rho=1}=0 \tag{56}$$

$$\frac{\partial Q_{\mathrm{N}}(\rho,\omega,\omega_0)}{\partial\rho}|_{\rho=1}=\frac{\sin\omega}{\cos\omega-\cos\omega_0} \tag{57}$$

$$\frac{\partial^2 Q_{\mathrm{N}}(\rho,\omega,\omega_0)}{\partial\rho^2}|_{\rho=1}=-\frac{\sin\omega}{\cos\omega-\cos\omega_0}\left[2\sin^2\omega+\frac{\cos(2\omega)}{4(\cos\omega-\cos\omega_0)^2}\right] \tag{58}$$

and (55) into (49) and truncating terms with orders higher than 3 yield (14).

Appendix B: Bandpass filter frequency response

A sinusoid whose frequency ω is identical to the notch frequency ω_0 will pass through the bandpass filter (3) without any amplitude change and phase shift. If the frequency ω is not equal but very close to ω_0, the sinusoid will pass through the bandpass filter with negligible amplitude and phase distortions. The bandpass filter response to the frequency ω that is far away from the notch frequency ω_0 is very important in investigating the role the bandpass filter plays in the ANFBs.

The frequency response is given by

$$A_{\mathrm{B}}(\omega,\omega_0)=|H_{\mathrm{B}}(e^{\nu\omega})| =(1-\rho)f_{\mathrm{B}}(\rho,\omega,\omega_0) \tag{59}$$

$$f_{\mathrm{B}}(\rho,\omega,\omega_0)= \sqrt{\frac{[-2\cos\omega_0\cos\omega+(1+\rho)\cos(2\omega)]^2+[2\cos\omega_0\sin\omega-(1+\rho)\sin(2\omega)]^2}{[1-2\rho\cos\omega_0\cos\omega+\rho^2\cos(2\omega)]^2+[2\rho\cos\omega_0\sin\omega-\rho^2\sin(2\omega)]^2}}. \tag{60}$$

Applying the Taylor series expansion to $f_{\mathrm{B}}(\rho,\omega,\omega_0)$ for $\rho=1$ leads to

$$f_{\mathrm{B}}(\rho,\omega,\omega_0)=f_{\mathrm{B}}(\rho,\omega,\omega_0)|_{\rho=1} -(1-\rho)\frac{\partial f_{\mathrm{B}}(\rho,\omega,\omega_0)}{\partial\rho}|_{\rho=1}+\cdots \tag{61}$$

Using

$$f_{\mathrm{B}}(\rho,\omega,\omega_0)|_{\rho=1}=\sqrt{1+\left(\frac{\sin\omega}{\cos\omega-\cos\omega_0}\right)^2} \tag{62}$$

$$\frac{\partial f_{\mathrm{B}}(\rho,\omega,\omega_0)}{\partial\rho}|_{\rho=1}=-\frac{1}{2}\left[1+\left(\frac{\sin\omega}{\cos\omega-\cos\omega_0}\right)^2\right]^{-\frac{1}{2}} \times\left[2+\frac{2\sin^2\omega-1+\cos\omega_0\cos\omega}{(\cos\omega-\cos\omega_0)^2}\right] \tag{63}$$

and (61) into (59) and including only the first Taylor series expansion term result in (15).

The phase response is given by

$$\phi_{\mathrm{B}}(\rho,\omega,\omega_0)=\tan^{-1}Q_{\mathrm{B}}(\rho,\omega,\omega_0) \tag{64}$$

$$Q_{\mathrm{B}}(\rho,\omega,\omega_0)=\frac{Q_{B_b}(\omega,\omega_0)Q_{N_c}(\rho,\omega,\omega_0)-Q_{B_a}(\omega,\omega_0)Q_{N_d}(\rho,\omega,\omega_0)}{Q_{B_a}(\omega,\omega_0)Q_{N_c}(\rho,\omega,\omega_0)+Q_{B_b}(\omega,\omega_0)Q_{N_d}(\rho,\omega,\omega_0)} \tag{65}$$

$$Q_{B_a}(\omega,\omega_0)=2\cos\omega_0\cos\omega-(1+\rho)\cos(2\omega) \tag{66}$$

$$Q_{B_b}(\omega,\omega_0)=-2\cos\omega_0\sin\omega+(1+\rho)\sin(2\omega). \tag{67}$$

Similarly, $Q_{\rm B}(\rho,\omega,\omega_0)$ may be expressed below by virtue of the Taylor series expansion with respect to ρ in the vicinity of one, as follows

$$Q_{\rm B}(\rho,\omega,\omega_0)=Q_{\rm B}(\rho,\omega,\omega_0)|_{\rho=1}-(1-\rho)\frac{\partial Q_{\rm B}(\rho,\omega,\omega_0)}{\partial\rho}|_{\rho=1} +\frac{1}{2}(1-\rho)^2\frac{\partial^2 Q_{\rm B}(\rho,\omega,\omega_0)}{\partial\rho^2}|_{\rho=1}+\cdots. \quad (68)$$

Substituting

$$Q_{\rm B}(\rho,\omega,\omega_0)|_{\rho=1}=-\frac{\sin\omega}{\cos\omega-\cos\omega_0} \quad (69)$$

$$\frac{\partial Q_{\rm B}(\rho,\omega,\omega_0)}{\partial\rho}|_{\rho=1}=\frac{1}{2}\frac{\sin\omega}{\cos\omega-\cos\omega_0} +\frac{1}{2}\frac{\sin\omega}{(\cos\omega-\cos\omega_0)^3}\left(1+\sin^2\omega-\cos\omega\cos\omega_0\right) \quad (70)$$

$$\frac{\partial^2 Q_{\rm B}(\rho,\omega,\omega_0)}{\partial\rho^2}|_{\rho=1}=\frac{3\sin\omega}{\cos\omega-\cos\omega_0}+\frac{5\sin\omega\cos\omega}{2(\cos\omega-\cos\omega_0)^2} +\frac{10\sin^3\omega+\sin\omega\cos^2\omega+4\sin\omega(1-\cos\omega\cos\omega_0)}{2(\cos\omega-\cos\omega_0)^3} +\frac{2\sin^3\omega\cos\omega}{(\cos\omega-\cos\omega_0)^4}+\frac{2\sin^5\omega}{(\cos\omega-\cos\omega_0)^5} \quad (71)$$

and (68) into (64) and truncating terms with orders higher than 3 yield (16).

Appendix C: Variance $\sigma^2_{C,i}$

If $i=1$, $\sigma^2_{C,1}$ is simply the variance of AWGN $v(n)$, i.e., $\sigma^2_{C,1}=\sigma^2$. If $i=2$, variance of the first ANF output noise $v_1(n)$ due to the input AWGN $v(n)$ may be obtained from [33]

$$\sigma^2_{C,2}=\frac{\sigma^2}{\rho^2}\left[1-\frac{1-\rho}{1+\rho}\frac{(1+\rho^2)(1+\rho)^2-8\rho^2\cos^2\omega_1}{\rho^4-2\rho^2\cos(2\omega_1)+1}\right] \approx\frac{1}{\rho^2}\left(1-2\frac{1-\rho}{1+\rho}\right)\sigma^2. \quad (72)$$

for a ρ that is very close to one. Clearly $\sigma^2_{C,2}$ is almost unrelated to the notch frequency ω_1.

Let us now verify if $v_1(n)$ still preserves the whiteness of its seed $v(n)$. Towards this end, one may compute the autocorrelation of $v_1(n)$ first by using the theory of residues

$$\begin{aligned} C_{or}(k) &= E[v_1(n)v_1(n-k)],\quad k\geq 1 \quad (73)\\ &=\frac{\sigma^2}{2\pi\nu}\oint_{\mathbf{c}} H_{N,1}(z)H_{N,1}(z^{-1})\frac{dz}{z^{k+1}}\\ &=\frac{\sigma^2}{2\pi\rho^2\nu}\oint_{\mathbf{c}}\frac{(z^2+c_1z+\rho^2)^2}{(z^2+\rho c_1z+1)(z^2+\frac{c_1}{\rho}z+\frac{1}{\rho^2})}\frac{dz}{z^{k+1}}\\ &=\frac{\sigma^2}{2\pi\rho^2\nu}\oint_{\mathbf{c}}\left(\sum_{j=1}^{4}\frac{\beta_j}{z-z_{1,j}}\right)\frac{dz}{z^{k+1}} \end{aligned}$$

where

$$z_{1,3} = \frac{1}{\rho}e^{\nu\omega_1},\quad z_{1,4}=\frac{1}{\rho}e^{-\nu\omega_1} \quad (74)$$

$$\beta_j = \frac{(z_{1,j}^2+c_1z_{1,j}+1)^2}{\prod_{m=1,m\neq j}^{4}(z_{1,j}-z_{1,m})},\quad j=1,2,3,4. \quad (75)$$

The residues for $z_{1,1}$, $z_{1,2}$, and $z_0\ (=0)$ are given by

$$Res(z_{1,1}) = \beta_1 z_{1,1}^{-(k+1)} \quad (76)$$

$$Res(z_{1,2}) = \beta_2 z_{1,2}^{-(k+1)} \quad (77)$$

$$Res(z_0) = -\sum_{j=1}^{4}\beta_j z_{1,j}^{-(k+1)}. \quad (78)$$

Finally, the autocorrelation is expressed by

$$C_{or}(k)=\frac{\sigma^2}{\rho^2}\left[Res(z_{1,1})+Res(z_{1,2})+Res(z_0)\right]. \quad (79)$$

Simulations have been conducted to compare the above theoretical expression and the simulated autocorrelation in terms of the autocorrelation coefficients (i.e., $C_{or}(k)/C_{or}(0)$) for several cases. Note that the theoretical expression (variance) $C_{or}(0)$ is used to compute the simulated autocorrelation coefficients in order to make the comparison fair and reliable between theory and simulations. Fig. 13 shows a comparison for a typical case where a very good fit is clearly observed between theory and simulations. Consequently, it has been demonstrated that the output of an ANF with respect to an AWGN input may be approximately regarded and treated as a white noise given that ρ is set close to 1, irrespective of the frequency the ANF targets. This finding implies that the equation (72) may be used to compute $\sigma^2_{C,3}$, as follows:

$$\begin{aligned}\sigma^2_{C,3} &\approx \frac{1}{\rho^2}\left(1-2\frac{1-\rho}{1+\rho}\right)\sigma^2_{C,2} \quad (80)\\ &\approx \left[\frac{1}{\rho^2}\left(1-2\frac{1-\rho}{1+\rho}\right)\right]^2\sigma^2.\end{aligned}$$

Therefore, for $i=1,2,\cdots,p$, one generally obtains

$$\sigma^2_{C,i} \approx \left[\frac{1}{\rho^2}\left(1-2\frac{1-\rho}{1+\rho}\right)\right]^{i-1}\sigma^2. \quad (81)$$

Acknowledgment

The authors would like to thank Mr. Masanori Makihara for coding some simulation programs used in this work. Constructive comments and suggestions of the anonymous reviewers have greatly helped improve presentation of this paper. This work was supported, in part, by the National Natural Science Foundation of China (51905453), the National Key R&D Program of China (2020YFB1200300ZL-03, 2018YFB1201603-14), the Science and Technology Project of Sichuan Province, China (2019JDRC0024), the Science and Technology Research and Development Program of China Railway Corporation (P2018J001), and the JSPS Grant-in-Aid for Scientific Research (C) (15K06117, 18K04175), Japan,

REFERENCES

[1] B. Widrow et al., "Adaptive noise cancelling: Principles and applications," *Proc. IEEE*, vol. 63, pp. 1692-1716, Dec. 1975.

[2] J. R. Treichler, "Transient and convergent behavior of the adaptive line enhancer," *IEEE Trans. ASSP*, vol. 27, pp. 53-62, Feb. 1979.

[3] D. W. Tufts and R. Kumaresan, "Estimating of frequencies of multiple sinusoids: Making linear prediction perform like maximum likelihood," *Proc. IEEE*, vol. 70, pp. 975-989, Sep. 1982.

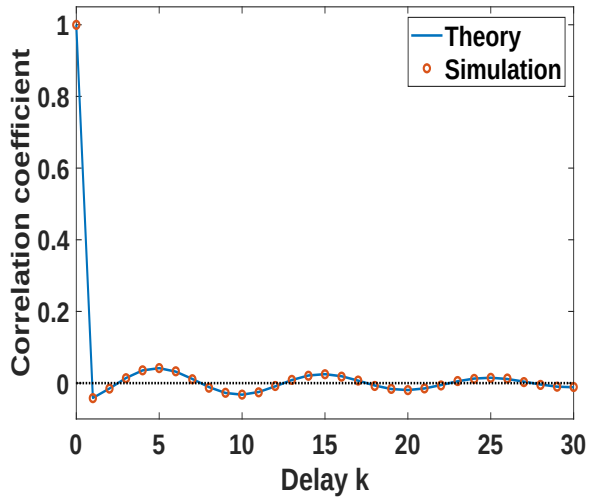

Fig. 13 Comparison between theoretical and simulated autocorrelation coefficients of the output noise for the first active cell in CANFB. ($\omega_1 = 0.2\pi$, $\sigma^2 = 0.5$, $\rho = 0.95$, 300 runs).

[4] D. B. Rao and Sun-Yuan Kung, "Adaptive notch filtering for the retrieval of sinusoids in noise," *IEEE Trans. ASSP*, vol. 32, no. 4, pp. 791-802, Aug. 1984.

[5] A. Nehorai, "A minimal parameter adaptive notch filter with constrained poles and zeros," *IEEE Trans. ASSP*, vol. 33, no. 4, pp. 983-996, Aug. 1985.

[6] N. I. Cho, C. H. Choi and S. U. Lee, "Adaptive line enhancement by using an IIR lattice notch filter," *IEEE Trans. ASSP*, vol. 37, no. 4, pp. 585-589, Apr. 1989.

[7] N. I. Cho and S. U. Lee, "On the adaptive lattice notch filter for the detection of sinusoids," *IEEE Trans. CAS.*, vol. 40, pp. 405-416, Jul. 1993.

[8] T. Kwan and K. Martin, "Adaptive detection and enhancement of multiple sinusoids using a cascade IIR filter," *IEEE Trans. CAS*, vol. 36, no. 7, pp. 937-947, Jul.1989.

[9] K. W. Martin and M. T. Sun, "Adaptive filters suitable for real-time spectral analysis," *IEEE Journal of Solid-State Circuits*, vol. 21, no. 1, pp. 108-119, Feb. 1986.

[10] J. F. Chicharo and T. S. Ng, "Gradient-based adaptive IIR notch filtering for frequency estimation," *IEEE Trans. ASSP*, vol. 38, no. 5, pp. 769-777, May 1990.

[11] T. Ng, "Some aspects of an adaptive digital notch filter with constrained poles and zeros," *IEEE Trans. ASSP*, vol. 35, no. 2, pp. 158-161, Feb. 1987.

[12] P. A. Regalia, "An improved lattice-based adaptive IIR notch filter," *IEEE Trans. Signal Process.*, vol. 39, no. 9, pp. 2124-2128, Sept. 1991.

[13] S. Pei and C. Tseng, "Adaptive IIR notch filter based on least mean p-power error criterion," *IEEE Trans. CAS-II*, vol. 40, no. 8, pp. 525-528, Aug. 1993.

[14] Y. Xiao,Y. Tadokoro and Y. Kobayashi, "A new memoryless nonlinear gradient algorithm for a second-order adaptive IIR notch filter and its performance analysis," *IEEE Trans. CAS-II*, vol. 45, no. 4, pp. 462-472, Apr. 1998.

[15] S. Pei and C. Tseng, "A novel structure for cascade form adaptive notch filters," *Signal Process.*, 33(1993), pp. 95-110, 1993.

[16] S. C. Pei and C. C. Tseng, "Real time cascade adaptive notch filter scheme for sinusoidal parameter estimation," *Signal Process.*, 39(1994), pp. 117-130, 1994.

[17] R. Punchalard, J. Koseeyapron, and P. Wardkein, "Adaptive IIR notch filter using a modified sign algorithm," *Signal Process.*, 89(2009), pp. 239-243, 2009.

[18] W. Loetwassana, R. Punchalard, J. Koseeyapron, and P. Wardkein, "Unbiased plain gradient algorithm for a second-order adaptive IIR notch filter with constrained poles and zeros," *Signal Process.*, 90(2010), pp. 2513-2520, 2010.

[19] R. Punchalard, "A modified inverse tangent based adaptive algorithm for a second-order constrained adaptive IIR notch filter," *Signal Process.*, 94(2014), pp. 350-358, 2014.

[20] H. Munakata, S. Koshita, M. Abe, and M. Kawamata, "Improvement of convergence speed for an adaptive notch filter based on simplified lattice algorithm using pilot notch filters," *IEEE Intl Conf Network Infrastructure & Digital Content (IC-NIDC)*, pp. 312-316, 2016.

[21] Y. Xiao, Y. Ma, and B. Huang, "A simplified variable step-size gradient algorithm for IIR notch filtering: Properties and application," *Intl Conf Advanced Mechatronic Systems (ICAMechS)*, pp. 78-82, 2017.

[22] R. Punchalard, "Bias mitigating in a sign-algorithm for a constrainted adaptive IIR notch filter," *7th Intl Electrical Engineering Congress (iEECON)*, pp. 1-4, 2019.

[23] W. Loedwassana, "Adaptive IIR notch filter with variable step size plain gradient algorithm based on error correlation governed by gradient accumulation," *17th Intl Conf Electrical Engineering/Electronics, Computer, Telecommunications & Information Technology (ECTI-CON)* , pp. 88-91, 2020.

[24] Y. Hinamoto and S. Nishimura, "Stability and bias analysis for adaptive normal state-space notch digital filters," *63rd Intl Midwest Sym Circuits & Systems (MWSCAS)*, pp. 166-169, 2020.

[25] Y Yuan, M. Qing, and H. Liang, "Average plain gradient based indirect frequency estimation using adaptive notch filter," *IEEE Canadian Conf Electrical & Computer Engineering (CCECE)*, pp. 1-5, 2020.

[26] Q. Lv and H. Qin, "A novel algorithm for adaptive notch filter to detect and mitigate the CWI for GNSS receivers," *IEEE 3rd Intl Conf Signal & Image Processing (ICSIP)*, pp. 444-451, 2018.

[27] S. W. Arif, A. Coskun, and I. Kale, "A fully adaptive lattice-based notch filter for mitigation of interference in GPS," *15th Conf Ph.D Research in Microelectronics & Electronics (PRIME)*, pp. 217-220, 2019.

[28] Z. Li, H. Xu, and Y. Wang, "Rotor bar fault diagnosis of squirrel cage asynchronous motors based on adaptive notch filters," *22nd Intl Conf Electrical Machines & Systems (ICEMS)*, pp. 1-4, 2019.

[29] J. R. Rivera-Guillen, J. J. de Santiago-Perez, J. P. Amezquita-Sanchez, et al., "Adaptive notch filter for induction motor condition monitoring," *IEEE Intl Autumn Meeting Power, Electronics & Computing (ROPEC)* , pp. 1-5, 2019.

[30] Z. Wang, Y. Xiao, L. Ma, K. Khorasani, and Y. Ma, "Multi-frequency narrowband active noise control with online feedback-path modeling using IIR adaptive notch filters," *IEEE Asia Pacific Conf Circuits & Systems (APCCAS)*, pp. 293-296, 2019.

[31] C. Y. Ho, K. K. Shyu, C. Y. Chang, and S. M. Kuo, "Efficient narrowband noise cancellation system using adaptive line enhancer," *IEEE Trans. Audio, Speech, Lan. Process.*,, vol. 28, pp. 1094-1103, 2020.

[32] B. Yu, H. Liu, and Y. Zhong, "Adaptive filtering method for removing engine interference frequency," *7th Intl Sym. Mechatronics & Industrial Informatics (ISMII)*, pp. 11-15, 2021.

[33] Y. Xiao, T. Takeshita, and K. Shida, "Steady-state analysis of a plain gradient algorithm for a second-order adaptive IIR notch filter with constrained poles and zeros," *IEEE Trans. Circuits Syst. II*, vol. 48, no. 7, pp. 733-740, July 2001.

[34] Y. Xiao, T. Matsuo, and K. Shida, "Modified constrained notch Fourier Transform (MCNFT) for sinusoidal signals in noise and its performance," *IEICE Trans Fundamentals*, vol. E85-A, no. 5, pp. 1096-1103, May 2002.

[35] Y. Xiao, R. K. Ward, L. Ma, and A. Ikuta, "A new LMS-based Fourier analyzer in the presence of frequency mismatch and applications," *IEEE Trans Circuits Syst. I*, vol. 52, no. 1, pp. 230-245, Jan. 2005.

[36] Y. Hu, B. Zhang, and A. Tan, "Acceleration signal with DTCWPT and novel optimize SNR index for diagnosis of misaligned cardan shaft in high-speed train," *Mechanical Systems and Signal Processing*, ISSN: 0888-3270, vol. 140, pp. 706-723, Feb. 2020.